

JOURNAL OF PHYSICAL SCIENCE

ISSN: 1675-3402 (PRINT) 2180-4230 (ONLINE)



USM
UNIVERSITI SAINS MALAYSIA



APEX™

PENERBIT
USM




PENYEBARAN ILMU MELALUI PENERBITAN

Editorial Board

Editor-in-Chief

- [Prof. Dr. Abdul Latif Ahmad \(Universiti Sains Malaysia\)](#) 

Editorial Board

- [Prof. Dr. Atsunori Matsuda \(Toyohashi University of Technology, Japan\)](#) 
- [Prof. Dr. Eiichiro Matsubara \(Kyoto University, Japan\)](#) 
- [Prof. Ulung Datuk Dr. Harith Ahmad \(University of Malaya, Malaysia\)](#) 
- [Prof. Dr. Hong-Wei Yen \(Tunghai University, Taiwan\)](#) 
- [Prof. Mark C. Bagley \(University of Sussex, United Kingdom\)](#) 
- [Prof. Nicolas Brosse \(University of Lorraine, France\)](#) 
- [Prof. Dr. Norli Ismail \(Universiti Sains Malaysia\)](#) 

Vol. 33, No. 3 (2022)

1. [Effect of Coupling Agent on Properties of Composites Made from Styrofoam Waste and Coconut Shell](#), by Koay Seong Chun, Subhramani Thangamuthu, Chan Ming Yeng and Ong Thai Kiat
2. [Fabrication of PES/PDMS/ZIF-L Composite Membrane for CO₂, N₂ and CH₄ Permeation](#), by Meor Muhammad Hafiz Shah Buddin and Abdul Latif Ahmad
3. [Performance Enhancement of Poly \(Vinyl Alcohol\) Composite Polymer Electrolyte for Li-Ion Battery Through Salt Immersion Process](#), by Christin Rina Ratri, Qolby Sabrina, Titik Lestariningsih and Salsabila Zakiiyah
4. [Simulation of Pt₈₀Au₁₄Ti₆ Work Function Change-Based Sensor of H₂ Gas](#), by Roniyus Marjunus, Yusril Al Fath, Yanti Yulianti and Wahyu Widanarto
5. [Synthesis and Characterisation of Graphene Oxide/Chitosan Composite Membranes from Natural Waste](#), by Andi Muhammad Afdhal Saputra, Nadea Agustina, Amran, Zurnansyah, Samnur and Eko Hadi Sujiono
6. [Calculating Microfield Angular Velocity Distribution in Plasma through Using Molecular Dynamics Simulation](#), by Abdallah Bekkouche and Fethi Khelfaoui
7. [Physiochemical and Electrochemical Properties of Lanthanum Strontium Cobalt Ferum–Copper \(II\) Oxide Prepared via Solid State Reaction](#), by Ahmad Fuzamy Mohd Abdul Fatah, Muhamad Nazri Murat and Noor Ashrina A. Hamid
8. [Effect of Rhombohedral and Spherical BiFeO₃ Catalyst on Biodiesel Production from Waste Cooking Oil](#), by Danny Lim Kay Wen, Nor Haida Mohd Kaus, Takaomi Kobayashi, Is Fatimah, Mohd Amirul Ramlan and Saifullahi Shehu Imam

Simulation of $\text{Pt}_{80}\text{Au}_{14}\text{Ti}_6$ Work Function Change-Based Sensor of H_2 Gas

Roniyus Marjunus,^{1*} Yusril Al Fath,¹ Yanti Yulianti¹ and Wahyu Widanarto²

¹Department of Physics, Faculty of Mathematics and Natural Sciences,
University of Lampung, Jl. Prof. Dr. Soemantri Brodjonegoro No.1,
Bandar Lampung 35145, Indonesia

²Department of Physics, Faculty of Mathematics and Natural Sciences, University of
Jenderal Soedirman, Jl. Prof. Dr. HR Boenyamin No.708, Dukuhbandong, Grendeng,
Kec. Purwokerto Utara, Kabupaten Banyumas 53122, Indonesia

*Corresponding author: roniyus.1977@fmipa.unila.ac.id

Published online: 30 November 2022

To cite this article: Marjunus, R. et al. (2022). Simulation of $\text{Pt}_{80}\text{Au}_{14}\text{Ti}_6$ work function change-based sensor of H_2 gas. *J. Phys. Sci.*, 33(3), 45–62. <https://doi.org/10.21315/jps2022.33.3.4>

To link to this article: <https://doi.org/10.21315/jps2022.33.3.4>

ABSTRACT: *Chemical reactions simulation in detecting hydrogen gas (H_2) on $\text{Pt}_{80}\text{Au}_{14}\text{Ti}_6$ sensor surface based on work function change ($\Delta\phi$) has been conducted. The simulation result is compared with laboratory results of detecting H_2 gas. Three chemical reactions contained three coverages, H coverage (θ_{H}), O coverage (θ_{O}), and H_2O coverage ($\theta_{\text{H}_2\text{O}}$). The simulation was run using MATLAB. This research can find the reaction parameter values such as the Arrhenius coefficient of H_2O forming reaction on Pt ($\mathcal{V}_{\text{FSPt}}$), H_2O forming reaction on Au (\mathcal{V}_{FAu}), i.e., H_2O dissociation on Au (\mathcal{V}_{FAu}), O_2 desorption on Ti ($\mathcal{V}_{\text{d2Ti}}$), H_2O forming reaction on Ti (\mathcal{V}_{FTi}), and H_2O dissociation on Ti (\mathcal{V}_{FTi}), i.e., $7.5 \times 10^{14} \text{ s}^{-1}$, $9.85 \times 10^{15} \text{ s}^{-1}$, $3.25 \times 10^{15} \text{ s}^{-1}$, $7.11 \times 10^{15} \text{ s}^{-1}$, $3.425 \times 10^{15} \text{ s}^{-1}$ and $2.725 \times 10^{15} \text{ s}^{-1}$, respectively. The simulation results also have the same trend as the laboratory results. However, the contact potential difference (CPD) simulation result, i.e., -240 mV , is not the same as the laboratory result, $(-297 \pm 9) \text{ mV}$. In addition, this simulation also obtained approximation coverage for atoms/molecules on $\text{Pt}_{80}\text{Au}_{14}\text{Ti}_6$ surface, i.e., $\theta_{\text{H}} = 0.665154 \text{ Mono Layer (ML)}$; $\theta_{\text{O}} = 1.5621 \times 10^{-6} \text{ ML}$; and $\theta_{\text{H}_2\text{O}} = 5.41676 \times 10^{-5} \text{ ML}$.*

Keywords: CPD, gas sensor, hydrogen, simulation, work function change

1. INTRODUCTION

Hydrogen (H) has been used in industry since the mid-20th century, such as a mixture of rocket fuel, hydrochloride production, iron ore reduction, fat hydrogenation and fuel cell.¹ H is the most abundant element, with 75% of the total air element. H is colourless, odourless, non-metallic, single valency and flammable at 4% concentrations in free air.² This gas is chemically active and rarely found in free form. H exists in compounds with other elements, such as oxygen in water (H₂O) or carbon in methane (CH₄). Hydrogen gas (H₂) will explode by itself at 560°C.³

The risk of using H could be minimised if a sensor gas could detect a gas leak. The gas sensor is a chemical sensor consisting of an active layer and transducer, which is used to convert chemical information into electronic signals such as current, frequency, and voltage.⁴ The capability of gas sensors depends on several parameters, such as sensitivity, selectivity, detection limit, response time and recovery time.⁵ There are two working mechanism types of gas sensors based on resistivity and work function change.⁶ The sensor uses the value of material work function change ($\Delta\phi$) caused by coming gases (also called contact potential difference/CPD) as the sensor signal. An example of a gas sensor based on a $\Delta\phi$ transducer is the floating gate field effect transistor (FGFET). The advantages of this method were the more straightforward process and fewer steps than other methods.⁷

Research on H₂ sensors has been carried out in platinum (Pt), nickel (Ni), titanium dioxide (TiO₂), zinc oxide (ZnO), palladium-gold alloy (PdAu), tin(IV) oxide (SnO₂) and Pt₈₀Au₁₄Ti₆.⁸⁻¹⁴ Research of H sensors using Pt₈₀Au₁₄Ti₆ based on CPD properties shows the signal (-297 ± 9) mV for 15,000 ppm H₂. Pt₈₀Au₁₄Ti₆ also has cross-sensitivity to the 50 ppm NH₃ and five ppm NO₂ with its signal, i.e., (100 ± 20) mV and (50 ± 10) mV.¹⁴ Another H₂ sensor which is using FGFET was also fabricated by Senft.¹⁵ Senft used Pt for the sensitive layer. The sensor signal is 600 mV for 20,000 ppm of H₂. When H₂ is increased linearly, the sensor signal raises logarithmic.

Three parameters are employed in the working mechanism of the gas sensor, i.e., the sticking coefficient, Arrhenius coefficient, and activation energy in each reaction. Since material parameter values are inferior, an optimisation process is needed to get the parameter's value.

The restriction is needed for the simulation in this study. It only uses three reactions between gas and material surface (H₂ adsorption, O₂ adsorption, and H and O reaction). No simulation has been carried out from the literature studies on this topic.

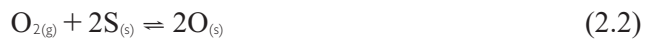
2. METHODS

2.1 Tools

The tool used in this study is a computer set with MATLAB software for simulations.

2.2 Reaction Mechanism

In research of H₂ detection in Pt, there are seven reactions between coming gases and material surface.⁸ Those reactions are written in Equation (2.1) to Equation (2.3). This simulation uses only three reactions, H₂ adsorption, O₂ adsorption and a reaction between H and O on the surface.



where S is the surface site. To calculate coverage (θ) change rate by gas on the surface in the adsorption process (atom/s or molecule/s) was started by calculating the adsorption rate in Equation (2.4).¹⁶

$$r_a = \frac{dN_{\text{ads}}}{dt} \quad (2.4)$$

N_{ads} is the number of atoms or molecules (on the surface), which could be defined in Equation (2.5).

$$N_{\text{ads}} = \sigma\theta \quad (2.5)$$

where σ is the surface atomic density of the layer (atom/m²), and θ is gas coverage on the surface (in Mono Layer or ML). The value of r_a also depends on the molecular flux in the material surface (F , m⁻² s⁻¹) based on Hertz-Knudsen law, as shown in Equation (2.6).¹⁶

$$F = -\frac{P}{\sqrt{2\pi mkT}} \quad (2.6)$$

Sticking probability (S , dimensionless) has presented in Equation (2.7).

$$S = S_0(1 - \theta)^\gamma \exp\left(-\frac{E_a}{kT}\right) \quad (2.7)$$

where P is gas pressure (Pa), m is the molecular gas mass (kg), k is Boltzmann constant (1.38×10^{-23} JK⁻¹), T is the temperature (K), S_0 is the initial sticking coefficient when coverage gas is still zero, and z is 1 for an undissociated gas and 2 for dissociated gas. According to Equation (2.6) and Equation (2.7), it can be seen that the temperature contributes to the calculation. The temperature contribution is not only in those equations but also for all the equations, which consist of activation energy. Then, if Equation (2.4) to Equation (2.7) are combined, gas θ rate change in the adsorption process is obtained as revealed in Equation (2.8).¹⁴

$$\frac{d\theta}{dt} = \frac{S_0(1-\theta)^z P}{\sigma \sqrt{2\pi mkT}} \exp\left(-\frac{E_a}{kT}\right) \quad (2.8)$$

When atoms or molecules of gas A (on the surface) are reacted with gas B (on the surface) to become AB molecules, based on the Langmuir-Hinshelwood mechanism, the θ rate of AB gas can be calculated using Equation (2.9).^{15,17}

$$\frac{d\theta_{AB}}{dt} = \nu_r \exp\left(-\frac{E_a}{kT}\right) \theta_A \theta_B \quad (2.9)$$

where ν_r is the Arrhenius coefficient or reaction frequency of A and B (reaction/s), E_r is the activation energy of the reaction between A and B gases (eV) and $\theta_A \theta_B$ is θ of A and B gases on the surface.

If a molecule (e.g., AB) dissociates into A and B (on the surface), then the θ rate change of gas A as given in Equation (2.10).¹⁵

$$\frac{d\theta_A}{dt} = \nu_{\text{diss}} \exp\left(-\frac{E_{\text{diss}}}{kT}\right) \theta_{AB} \quad (2.10)$$

where ν_{diss} is the Arrhenius coefficient or dissociation frequency AB (dissociation/s), E_{diss} is AB dissociation energy (eV), and θ_{AB} is AB molecule coverage.

Adsorbed molecules on the surface will be rereleased when given the desorption energy (E_d in eV). θ rate change can be determined using Equation (2.11).¹⁴

$$\frac{d\theta}{dt} = \nu_d \exp\left(-\frac{E_d}{kT}\right) \theta \quad (2.11)$$

where ν_d is the Arrhenius coefficient or desorption frequency (desorption/s).

Afterwards, the work function (ϕ) of the material depends on the gas θ . The work function of Pt has already been known as presented in Equation (2.12) to Equation (2.15).¹⁸⁻²⁰

$$\phi_{\text{H-Pt}} = -0.23\theta_{\text{H}}^{4/3} \text{ eV} \quad (2.12)$$

$$\phi_{O-Pt} = 2.663\theta_o \text{ eV, if } \theta_o < 0.0086 \text{ ML} \quad (2.13)$$

$$\phi_{O-Pt} = (0.557\theta_o + 0.184) \text{ eV, if } \theta_o \geq 0.0086 \text{ ML} \quad (2.14)$$

$$\phi_{H_2O-Pt} = (-1.1798\theta_{H_2O}^3 + 3.3114\theta_{H_2O}^2 - 1.1798\theta_{H_2O} - 0.0108) \text{ eV} \quad (2.15)$$

In Gottfried's research, the work function of Au with oxygen gas was formulated in Equation (2.16).²¹

$$\phi_{O-Au} = \frac{1.7 \times 10^{19} \times 3.3 \times 10^{-30} \theta_o}{8.85 \times 10^{12} (1 + 9 \times 1.5 \times 10^{-24} \times 10^{-6} \times (1.7 \times 10^{19} \theta_o))} \text{ eV} \quad (2.16)$$

For Ti material, work function formula (ϕ) of O and H₂O as given in Equation (2.17) and Equation (2.18).^{22,23}

$$\phi_{O-Ti} = 0.586\theta_o - 0.0415 \text{ eV} \quad (2.17)$$

$$\phi_{H_2O-Ti} = -0.49\theta_{H_2O} \text{ eV} \quad (2.18)$$

Since ϕ_{H-Au} , ϕ_{H_2O-Au} and ϕ_{H-Ti} are not available, the work function value was made equal to coverage (θ) as revealed in Equation (2.19) to Equation (2.21),

$$\phi_{H-Au} = \theta_{H-Au} \text{ eV} \quad (2.19)$$

$$\phi_{H_2O-Au} = \theta_{H_2O-Au} \text{ eV} \quad (2.20)$$

$$\phi_{H-Ti} = \theta_{H-Ti} \text{ eV} \quad (2.21)$$

Because Pt₈₀Au₁₄Ti₆ is a mixture of three materials, the work function of each material is as written in Equation (2.22) – Equation (2.24),

$$\phi_{Pt} = \phi_{H-Pt} + \phi_{O-Pt} + \phi_{H_2O-Pt} \quad (2.22)$$

$$\phi_{Au} = \phi_{H-Au} + \phi_{O-Au} + \phi_{H_2O-Au} \quad (2.23)$$

$$\phi_{Ti} = \phi_{H-Ti} + \phi_{O-Ti} + \phi_{H_2O-Ti} \quad (2.24)$$

Then, the total work function value (ϕ_{Total}) is based on the percentage of each material as given in Equation (2.25).

$$\phi_{Total} = 80\%\phi_{Pt} + 14\%\phi_{Ti} + 6\%\phi_{Ti} \quad (2.25)$$

Finally, the relation between work function and CPD is written in Equation (2.26).²⁴

$$CPD = \frac{\phi_{\text{Total}}}{|e|} \quad (2.26)$$

2.3 Fitting of Experimental Graph

Before the parameter optimisation process is carried out, it is necessary to approach the experimental graph of Marjunus with fitting.¹⁴ It calculates the error between the simulation and the experimental results.

2.4 Parameter Optimisation

The simulation requires 36 parameters for the H₂ gas detection process, as shown in Table 1.²⁵⁻⁴⁴ The six parameters were Arrhenius coefficients i.e., v_{fPt} , v_{fAu} , v_{r3Au} , v_{d2Ti} , v_{fTi} and v_{r3Ti} . Their values would be obtained by finding the smallest error average value between the simulation and the experimental results. However, six parameters are unknown, so an optimisation process was needed to get the best deal.

Table 1. Data of H₂ gas detection parameter on Pt₈₀Au₁₄Ti₆ surface.

S ₀ dan Arrhenius coefficient (s ⁻¹)		Activation energy (eV)	
Forward reaction	Reverse reaction	Forward reaction	Reverse reaction
$S_{01\text{Pt}} = 0.046$	$v_{\text{d1Pt}} = 6.0 \times 10^{12}$	$E_{\text{f1Pt}} = 0.13$	$E_{\text{r1Pt}} = 0.91$
$S_{02\text{Pt}} = 0.07 \times (300/T)$	$v_{\text{d2Pt}} = 8.0515 \times 10^{12}$	$E_{\text{f2Pt}} = 0.53$	$E_{\text{r2Pt}} = 2.20 - 966.0622\theta_0$
$v_{\text{fPt}} = -$	$v_{\text{r3Pt}} = 3.1 \times 10^{15}$	$E_{\text{f3Pt}} = 0.42$	$E_{\text{r3Pt}} = 0.68$
$S_{01\text{Au}} = 0.5$	$v_{\text{d1Au}} = 1.0 \times 10^{13}$	$E_{\text{f1Au}} = 0.16$	$E_{\text{r1Au}} = 0.68$
$S_{02\text{Au}} = 0.005$	$v_{\text{d2Au}} = 1.0 \times 10^{11}$	$E_{\text{f2Au}} = 2.17$	$E_{\text{r2Au}} = 1.6$
$v_{\text{fAu}} = -$	$v_{\text{r3Au}} = -$	$E_{\text{f3Au}} = 0.92$	$E_{\text{r3Au}} = 2.3$
$S_{01\text{Ti}} = 0.17$	$v_{\text{d1Ti}} = 2.1 \times 10^7$	$E_{\text{f1Ti}} = 0.5$	$E_{\text{r1Ti}} = 0.51$
$S_{02\text{Ti}} = 0.62$	$v_{\text{d2Ti}} = -$	$E_{\text{f2Ti}} = 1.15$	$E_{\text{r2Ti}} = 0.152$
$v_{\text{fTi}} = -$	$v_{\text{r3Ti}} = -$	$E_{\text{f3Ti}} = 1.09$	$E_{\text{r3Ti}} = 1.10$

2.5 Re-optimisation Parameters

After the value of v_{fPt} , v_{fAu} , v_{r3Au} , v_{d2Ti} , v_{fTi} , and v_{r3Ti} were obtained, the re-optimisation process was required for them to check the change value of each parameter. If the value was changed, the final value was acquired by the initial optimisation and re-optimisation average.

2.6 Final Simulation

The final process of this research was simulating all parameters that have been optimised. The final values of all parameters were entered into the program to simulate Matlab. This step obtained θ value, total work function (ϕ_{Total}), and *CPD*. *CPD* (V) graph would be plotted against time (t), and then *the CPD* graph was compared with Marjunus's laboratory result.¹⁴

3. RESULTS AND DISCUSSION

3.1 Differential Equation

This simulation used three reactions: H₂ adsorption, O₂ adsorption, and H with O reactions, Equation (2.12) to Equation (2.14). Those reactions were made into the coupled first order ordinary differential equations as written in Equation (4.1) to Equation (4.3) to obtain coverage value (θ), work function change ($\Delta\phi$), and *CPD*.

$$\frac{d\theta_{\text{H}}}{dt} = r_{\text{f1}}F_{\text{H2}} - r_{\text{b3}}\theta_{\text{H}}^2\theta_{\text{O}} + r_{\text{f3}}\theta_{\text{H2O}} - r_{\text{f1}}\theta_{\text{H}}^2 \quad (3.1)$$

$$\frac{d\theta_{\text{O}}}{dt} = 2r_{\text{f2}}F_{\text{O2}} - r_{\text{b3}}\theta_{\text{H}}^2\theta_{\text{O}} + r_{\text{f3}}\theta_{\text{H2O}} - 2r_{\text{f2}}\theta_{\text{O}}^2 \quad (3.2)$$

$$\frac{d\theta_{\text{H2O}}}{dt} = r_{\text{b3}}\theta_{\text{H}}^2\theta_{\text{O}} - r_{\text{f3}}\theta_{\text{H2O}} \quad (3.3)$$

where F is the adsorption factor, and r is the gas θ rate described in Equation (3.4) to Equation (3.6).¹⁵

$$F_x = (1 - \theta_x)^z \frac{P}{\sqrt{2\pi mkT}} \quad (3.4)$$

$$r_{\text{f}} = S_{\text{ox}} \exp\left(-\frac{E_{\text{f}}}{kT}\right) \quad (3.5)$$

$$r_{\text{for r}} = \nu_{\text{f or r}} \exp\left(-\frac{E_{\text{f}}}{kT}\right) \quad (3.6)$$

where x index in Equation (3.4) represents the symbol of coming gases at Pt₈₀Au₁₄Ti₆ surface, z is 1 for undissociated gas and 2 for dissociated gas, P is gas pressure (Pa), m is gas mass (kg), k is Boltzman constant, T is the temperature (K), and σ is atomic density on the surface (value for Pt, Au and Ti are 1.3×10^{19} atom/m², 1.2×10^{19} atom/m², and 2.3×10^{19} atom/m², respectively).¹⁴ Equation (3.5) was only used to find the (θ) rate of the H₂ and O₂ adsorption process (forward reaction of Equation [2.2] and Equation [2.3]). Equation (3.6) was used to calculate the θ rate except H₂ and O₂ gas adsorption process. Index f in Equation (3.5) and

Equation (3.6) describes the forward reaction, r index in Equation (3.6) represents the reverse reaction.

3.2 Fitting of Experimental Graph

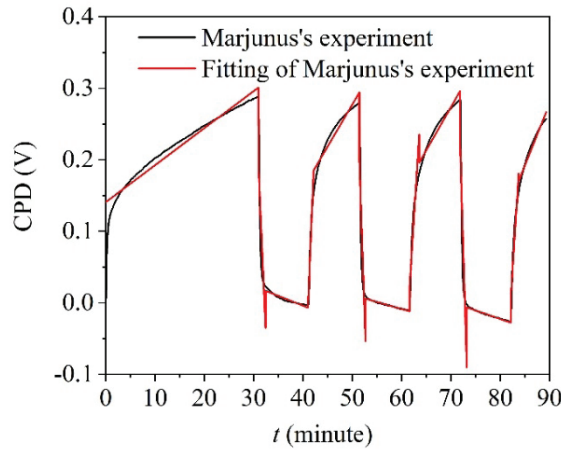


Figure 1: Fitting of Marjunus's graph.¹⁴

The fitting graph is presented in Figure 1. Each trend graph was fitted with has R-Square (COD) value which described the correlation factor between the laboratory result and its fitting. The average R-Square (COD) value is 0.89518, which is confirmed that the fitting curve approaches with laboratory results.

3.3 Parameter Optimisation Results

After the fitting process was completed, six parameters (v_{f3Pt} , v_{f3Au} , v_{r3Au} , v_{d2Ti} , v_{f3Ti} , and v_{r3Ti}) were optimised to find values with the smallest CPD error of those parameters. Before the optimisation process starts, the initial values must be given to those parameters. The results of optimisation are presented in Figure 2 to Figure 7.

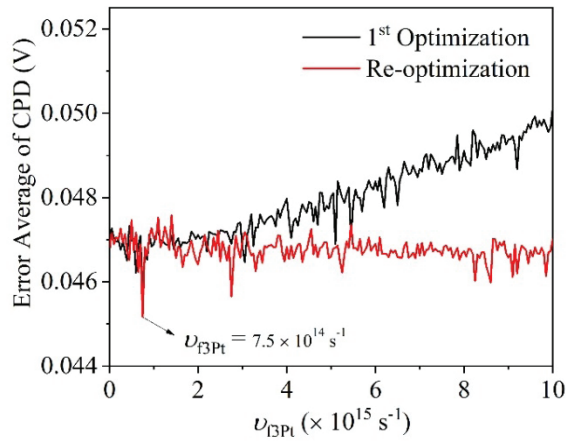


Figure 2: Optimisation of v_{f3Pt} with $5 \times 10^{13} \text{ s}^{-1}$ partition length.

Figure 2 shows the initial optimisation and re-optimisation of the Arrhenius coefficient of the H_2O forming reaction on Pt (v_{f3Pt}). The smallest error average (0.045169 V) of the initial optimisation occurs at the exact value of v_{f3Pt} of the re-optimisation, i.e., at $7.5 \times 10^{14} \text{ s}^{-1}$.

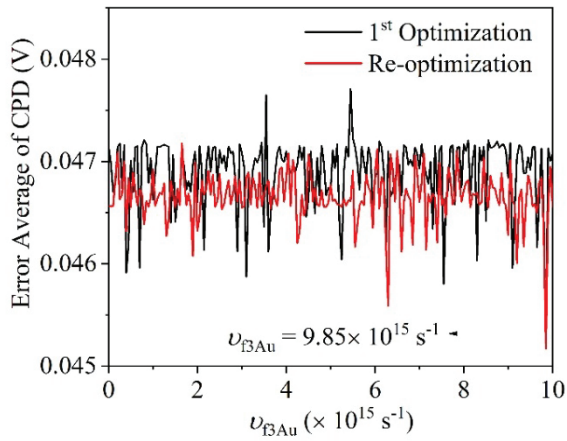


Figure 3: Optimisation of v_{f3Au} with $5 \times 10^{13} \text{ s}^{-1}$ partition length.

Then, the smallest error average (0.045169 V) of the initial optimisation and re-optimisation of H₂O forming reaction on Au (v_{r3Pt}) occurs also at the same value, i.e., $9.85 \times 10^{15} \text{ s}^{-1}$ (Figure 3).

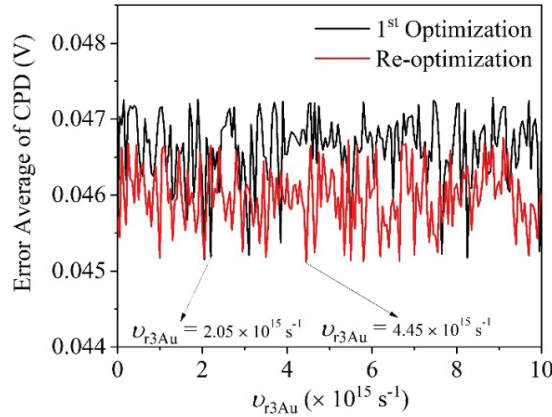


Figure 4: Graphic optimisation for with $5 \times 10^{13} \text{ s}^{-1}$ partition length.

On the other hand, Figure 4 presents the different values for Arrhenius coefficient dissociation of H₂O on Au (v_{r3Au}) at the initial optimisation and re-optimisation (at the smallest error average), i.e., $4.45 \times 10^{15} \text{ s}^{-1}$ and $2.05 \times 10^{15} \text{ s}^{-1}$. The average/final value for v_{r3Au} is $3.25 \times 10^{15} \text{ s}^{-1}$.

The same properties as v_{r3Au} also happen for the Arrhenius coefficient of:

1. O₂ desorption on Ti (v_{d2Ti}), the initial optimisation and re-optimisation values are $6.88 \times 10^{14} \text{ s}^{-1}$ and $7.34 \times 10^{14} \text{ s}^{-1}$, respectively, which gives the average, i.e., $7.11 \times 10^{14} \text{ s}^{-1}$ (Figure 5).
2. H₂O forming reaction on Ti (v_{r3Ti}), the initial optimisation and re-optimisation values are $5.65 \times 10^{15} \text{ s}^{-1}$ and $1.2 \times 10^{15} \text{ s}^{-1}$, respectively, which results in the average value at $3.425 \times 10^{15} \text{ s}^{-1}$ (Figure 6).
3. In dissociation of H₂O on Ti (v_{r3Ti}), the initial optimisation and re-optimisation values are $2.35 \times 10^{15} \text{ s}^{-1}$ and $3.1 \times 10^{15} \text{ s}^{-1}$, respectively, which results in the average value at $2.725 \times 10^{15} \text{ s}^{-1}$ (Figure 7).

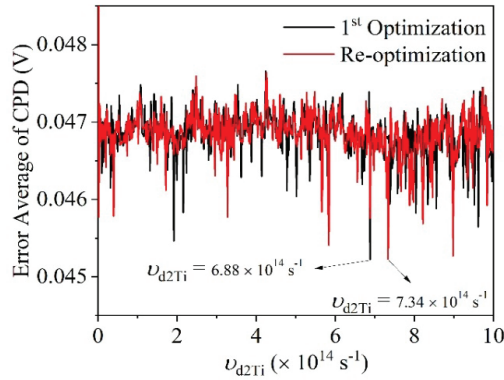


Figure 5: Graphic optimisation for v_{d2Ti} with $2 \times 10^{12} \text{ s}^{-1}$ partition length.

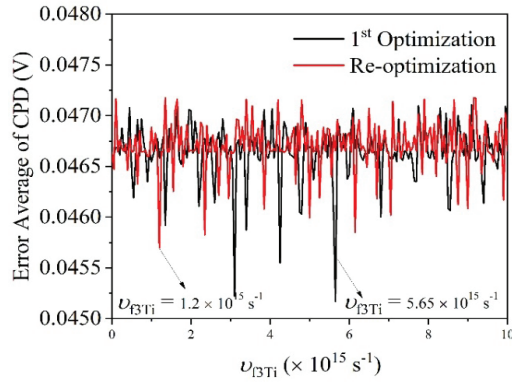


Figure 6: Graphic optimisation for v_{t3Ti} with $5 \times 10^{13} \text{ s}^{-1}$ partition length.

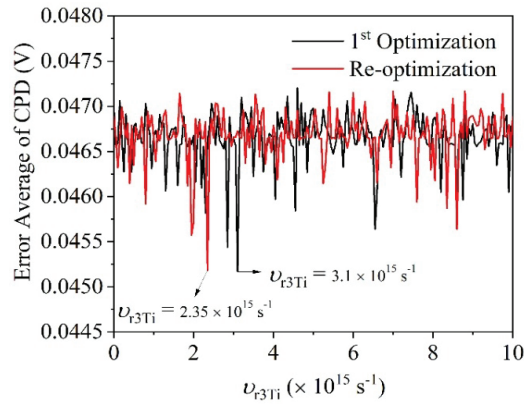


Figure 7: Graphic optimisation for v_{t3Ti} with $5 \times 10^{13} \text{ s}^{-1}$ partition length.

The parameter values invented in this work (Table 2) complete the previous research from other scientists, as presented in Table 1. The recapitulation of those values is shown in Table 2. These values are one of the primary inventions of this research. After these values are obtained, it means that all of the parameter values which are needed for the final simulation are available.

Table 2. The final value of six parameters after initial optimisation and re-optimisation.

Parameter	Initial Optimisation (s ⁻¹)	Re-optimisation (s ⁻¹)	Final value (s ⁻¹)
v_{Pt}	7.5×10^{14}	7.5×10^{14}	7.5×10^{14}
v_{Au}	9.85×10^{15}	9.85×10^{15}	9.85×10^{15}
v_{Au}	2.05×10^{15}	4.45×10^{15}	3.25×10^{15}
v_{Ti}	6.88×10^{14}	7.34×10^{14}	7.11×10^{14}
v_{Ti}	5.65×10^{15}	1.2×10^{15}	3.425×10^{15}
v_{Ti}	3.1×10^{15}	2.35×10^{15}	2.725×10^{15}

3.4 Final Simulation

After four steps in this research have been completed, the final process is the final simulation. The final simulation is a computation involving all parameter values from the literature study and this research. The CPD graph in this process will be compared with Marjunus's laboratory result.¹⁴ The result is shown in Figure 8. According to Figure 8, in Marjunus's research, CPD change of Pt₈₀Au₁₄Ti₆ when 15,000 ppm H₂ gas is exposed on the surface sample, i.e., (-297 ± 9) mV.¹⁴ Based on the simulation results, the CPD change of Pt₈₀Au₁₄Ti₆ is -240 mV, which means there is still a tiny difference between the simulation and laboratory results. But this simulation seems successful because the trend of simulation results is almost the same as the laboratory result.

Additionally, Figure 8 also shows the response and recovery time of the sensor signal. It proves again that the simulation result confirms the laboratory signal. The response/recovery time of simulation results is in agreement with the laboratory signals. When the H₂ is switched on, the laboratory and simulation signal decrease immediately. However, the laboratory signals are not saturated as the simulation signal, the laboratory signal increases as well as the simulation signal when the H₂ is switched off.

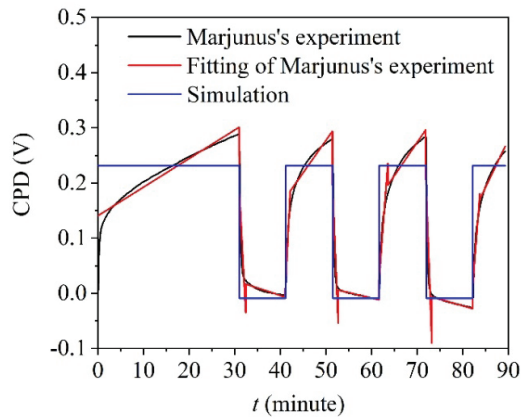
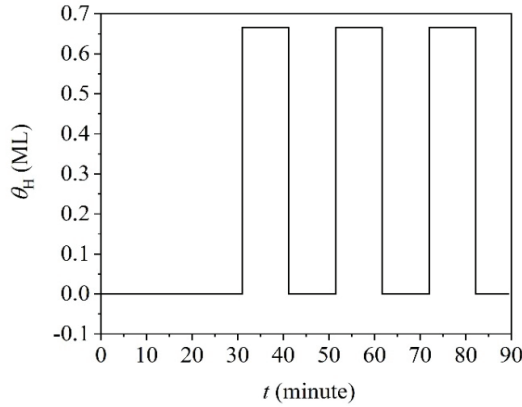


Figure 8: Comparison of H_2 signal sensor simulation and Marjunus's experiment.¹⁴

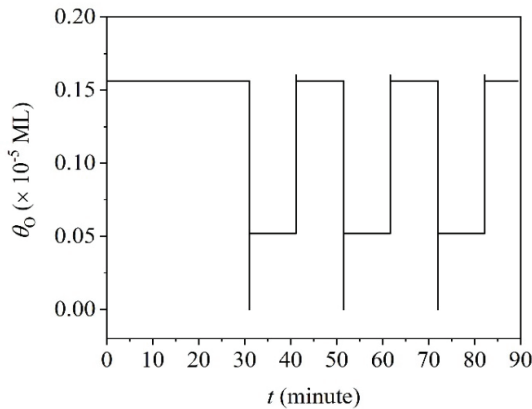
Several factors that cause the difference in CPD between simulation and laboratory results are as follows:

- The involved gases in the simulation process are still incomplete.
- Three involved reactions in the simulation process are fewer than in reality (experiments).
- There are still three of nine work function (ϕ) formulations that are unknown, so those formulations are approached as presented in Equation (2.19) to Equation (2.21).

Furthermore, another advantage of this simulation is calculating the atoms/molecules of gases on the surface of $Pt_{80}Au_{14}Ti_6$. H coverage (θ_H) on the surface during the gas detection process can be seen in Figure 9.

Figure 9: θ_H on $\text{Pt}_{80}\text{Au}_{14}\text{Ti}_6$ surface.

Based on Figure 9, θ_H increases until 0.67 ML when H_2 gas is exposed. It can be understood because when the H_2 gas is adsorbed on the $\text{Pt}_{80}\text{Au}_{14}\text{Ti}_6$ surface, it will be dissociated into two atoms of H, see Equation (2.1). The H atom coverage will decrease again to zero if the H_2 gas is switched off.

Figure 10: Coverage of oxygen atom (θ_O) on $\text{Pt}_{80}\text{Au}_{14}\text{Ti}_6$ surface.

Then, the θ_O on the $\text{Pt}_{80}\text{Au}_{14}\text{Ti}_6$ surface is presented in Figure 10. According to Figure 10, the maximum coverage of the oxygen atom on the $\text{Pt}_{80}\text{Au}_{14}\text{Ti}_6$ surface is 1.6×10^{-6} ML. The oxygen coverage decreases when the H_2 gas is exposed. It can be explained by Equation (2.2) and Equation (2.3). When the oxygen gas comes to the $\text{Pt}_{80}\text{Au}_{14}\text{Ti}_6$ surface, it will be dissociated to be two atoms of oxygen, Equation (2.2). Then each oxygen atom on the $\text{Pt}_{80}\text{Au}_{14}\text{Ti}_6$ surface will react with two adsorbed atoms of H-producing water molecules on the $\text{Pt}_{80}\text{Au}_{14}\text{Ti}_6$

surface, which decreases the occupation of the oxygen atom on the $\text{Pt}_{80}\text{Au}_{14}\text{Ti}_6$ surface. Based on Figure 10, the oxygen coverage is not as much as H coverage (Figure 9). Still, oxygen coverage has more influence on the work function of $\text{Pt}_{80}\text{Au}_{14}\text{Ti}_6$ because oxygen is a gas that interacts firstly with the surface of $\text{Pt}_{80}\text{Au}_{14}\text{Ti}_6$. It means oxygen changes the work function of $\text{Pt}_{80}\text{Au}_{14}\text{Ti}_6$ at the beginning of the process. Once the oxygen coverage decreases because of the reaction with the incoming H, it causes the work function change of $\text{Pt}_{80}\text{Au}_{14}\text{Ti}_6$.

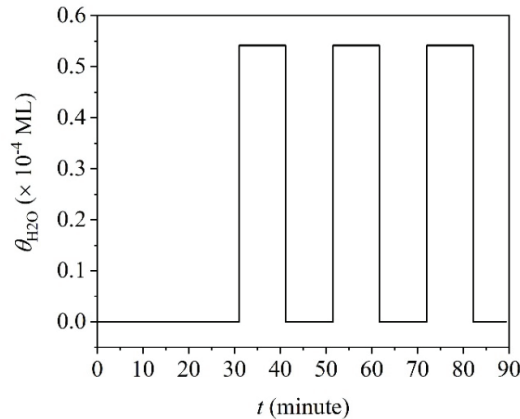


Figure 11: Coverage of water molecule ($\theta_{\text{H}_2\text{O}}$) on $\text{Pt}_{80}\text{Au}_{14}\text{Ti}_6$ surface.

Finally, this simulation can also calculate the $\theta_{\text{H}_2\text{O}}$ on the $\text{Pt}_{80}\text{Au}_{14}\text{Ti}_6$ surface (Figure 11). Based on Figure 11, the water molecule coverage starts with zero. It will not be zero if the adsorption of a water molecule in the air takes place in the calculation. Afterwards, the water molecule coverage increases along with the exposure of H_2 gas because the adsorbed-oxygen atom and the adsorbed-H molecules react with each other, producing adsorbed-water molecules until $5.4 \times 10^{-5} \text{ ML}$.

4. CONCLUSION

This research successfully obtains the unknown values of six parameters of H_2 gas detection through optimisation and simulation of the detection process by using MATLAB. This simulation can approach the graphic trend of experimental results with a very good approximation. The height of the simulated signal (-240 mV) is also almost close to the experimental signal ($-297 \pm 9 \text{ mV}$). Other contributions of this study, i.e., it can predict the occupation/coverage of atoms/molecules of gases on the $\text{Pt}_{80}\text{Au}_{14}\text{Ti}_6$ surface, which another experiment in the laboratory should prove.

5. REFERENCES

1. Zore, U. K. et al. (2021). A review on recent advances in hydrogen energy, fuel cell, biofuel and fuel refining via ultrasound process intensification. *Ultrason. Sonochem.*, 73, 105536. <https://doi.org/10.1016/j.ultsonch.2021.105536>
2. Yang, L. et al. (2014). A study of hydrogen sensing properties and microstructure for highly dispersed Pd SnO₂ thin films with high response magnitude. *App. Surf. Sci.*, 311, 74–82. <https://doi.org/10.1016/j.apsusc.2014.05.003>
3. Reece, J. B. et al. (2011). The chemical context of life. In J. B. Reece (10th Ed.). *Campbell Biology 10th Edition*. London: Pearson.
4. Yunusa, Z. et al. (2014). Gas Sensors: A Review, *Sens.*, 168, 61–75.
5. Hübert, T. et al. (2011). Hydrogen sensors – A review. *Sens. Actuators B Chem.*, 157, 2, 329–352. <https://doi.org/10.1016/j.snb.2011.04.070>
6. Gu, H. et al. (2012). Hydrogen gas sensors based on semiconductor oxide nanostructures. *Sens.*, 12(5), 5517–5550. <https://doi.org/10.3390/s120505517>
7. Korotcenkov, G. (2013). *Handbook of Gas Sensor Material: Properties, Advantages and Shortcomings for Application Volume 1 Conventional Approaches*. New York: Springer, 1–45.
8. Senft, C. et al. (2012). Theory and application of suspended gate FET gas sensors. *Chem. Sens. and Biosens.*, 11, 79–112. https://doi.org/10.1007/5346_2011_12
9. Pour, G. B. et al. (2018). Sensitive capacitive-type hydrogen sensor based on Ni thin film in different hydrogen concentrations. *Curr. Nanosci.*, 14(2), 136–142. <https://doi.org/10.2174/1573413713666171002124909>
10. Li, Z. et al. (2018). Resistive-type hydrogen gas sensor based on TiO₂: A review. *Int. J. Hydrog. Energy*, 43(45), 21114–21132. <https://doi.org/10.1016/j.ijhydene.2018.09.051>
11. Abdulgafour, H. I. et al. (2016). Hydrogen gas sensor based on ZnO nanorods grown on Si by thermal evaporation, *Mater. Sci. Eng. A*, 6(3–4), 51–56. <https://doi.org/10.17265/2161-6213/2016.3-4.002>
12. Pak, Y. et al. (2018). Highly stable and ultrafast hydrogen gas sensor based on 15 nm nanogaps switching in a palladium–gold nanoribbons array. *Adv. Mater. Interfaces*, 6(4), 1–9. <https://doi.org/10.1002/admi.201801442>
13. Kadhim, I. H. et al. (2016). Hydrogen gas sensor based on nanocrystalline SnO₂ thin film grown on bare Si substrates. *Nanomicro Lett.*, 8(1), 20–28. <https://doi.org/10.1007/s40820-015-0057-1>
14. Marjunus, R. (2018). *Development of Pt-Based Sensitive Layer for Carbon Monoxide Work Function Change Based Sensor in Air Temperatur*, PhD diss., Universität der Bundeswehr, Munchen.
15. Senft, C. (2009). *Austrittsarbeitsbasierte Wassertofdetektion für Fahrzeuge mit Brennstoffzellenantrieb*. PhD diss., Universität der Bundeswehr, Munchen.
16. Somorjai, G. A. & Li, Y. (2010). *Introduction to Surface Chemistry and Catalysis Second Edition*. New Jersey: John Wiley & Son.
17. Yan, X. T. & Yu, X. (2010). *Chemical Vapor Deposition*. Berlin: Springer.
18. Christmann, K. et al. (1976). Adsorption of hydrogen on a Pt(111) surface. *Surf. Sci.*, 54(2), 386–392. [https://doi.org/10.1016/0039-6028\(76\)90232-6](https://doi.org/10.1016/0039-6028(76)90232-6)

19. Derry, G. N. & Ross, P. N. (1985). A work function change study of oxygen adsorption on Pt(111) and Pt(100). *J. Chem. Phys.*, 82(6), 2772–2778. <https://doi.org/10.1063/1.448274>
20. Heinzinger, K. (1991). Molecular dynamics studies of platinum/water interfaces. *Pure Appl. Chem.*, 63(12), 1733–1742. <https://doi.org/10.1351/pac199163121733>
21. Gottfried, J. M. (2003). *CO Oxidation Over Gold: Adsorption and Reaction of Oxygen, Carbon Monoxide, and Carbon Dioxide on an Au(110)-(1x2) surface*. PhD diss., Universität Berlin.
22. Jonker, B. T. et al. (1981). Surface states and oxygen chemisorption on Ti(0001). *Phys. Rev. B*, 24, 2951–2957. <https://doi.org/10.1103/PhysRevB.24.2951>
23. Bundaleski, N. et al. (2010). Adsorption dynamics of water on the surface of TiO₂ (110). *J. Phys. Conf. Ser.*, 257, 12008. <https://doi.org/10.1088/1742-6596/257/1/012008>
24. Vilitis, O. et al. (2016). Determination of contact potential difference by the Kelvin Probe (Part I) I. Basic principles of measurements. *Latv. J. Phys. Tech.*, 53(2), 48–57. <https://doi.org/10.1515/lpts-2016-0013>
25. Koop, J. & Deutschmann, O. (2009). Detailed surface reaction mechanism for Pt-catalyzed abatement of automotive exhaust gases. *Appl. Catal. B*, 91(1–2), 47–58. <https://doi.org/10.1016/j.apcatb.2009.05.006>
26. Callaghan, C. A. (2006). *Kinetic and Catalysis of Water-Gas-Shift Reaction: A Microkinetic and Graph Theoretic Approach*. PhD diss., Worcester Polytechnic Institute.
27. Behrendt, F. (1999). *Experimentelle und Numerische Beschreibung Katalytischer Zund und Verbrennungsprozesse*. Habilitationsschrift, Fakultät für Energietechnik der Universität Stuttgart.
28. Matsuda, K. & Harada, S. (2005). Dynamical desorption process of oxygen on platinum by using a gas controllable H₂ | H+Electrolyte | Pt cell. *Mater. Trans.*, 46(5), 1058–1063. <https://doi.org/10.2320/matertrans.46.1058>
29. Picolin, A. et al. (2009). Desorption of H₂O from flat and stepped Pt(111). *J. Phys. Chem. C*, 113, 691–697. <https://doi.org/10.1021/jp808170f>
30. Michaelides, A. & Hu, P. (2001). Catalytic water formation on platinum: A first-principles study. *J. Am. Chem. Soc.*, 123, 4235–4242. <https://doi.org/10.1021/ja003576x>
31. Winkler, A. (1998). Interaction of atomic hydrogen with metal surfaces. *Appl. Phys. A*, 67, 637–644. <https://doi.org/10.1007/s003390050835>
32. Pan, M. et al. (2013). Model studies of heterogeneous catalytic hydrogenation reactions with gold. *Chem. Soc. Rev.*, 42, 5002–5013. <https://doi.org/10.1039/C3CS35523C>
33. Linsmeier, C. & Wanner, J. (2000). Reactions of oxygen atoms and molecules with Au, Be, and W surfaces. *Surf. Sci.*, 454, 305–309. [https://doi.org/10.1016/S0039-6028\(00\)00215-6](https://doi.org/10.1016/S0039-6028(00)00215-6)
34. Gottfried, J. M. et al. (2002). Spontaneous and electron-induced adsorption of oxygen on Au(110)-(1×2). *Surf. Sci.*, 511(1–3), 65–82. [https://doi.org/10.1016/S0039-6028\(02\)01555-8](https://doi.org/10.1016/S0039-6028(02)01555-8)

35. Chester, M. A. & Somorjai, G. A. (1975). The chemisorption of oxygen, water, and selected hydrocarbons on the (111) and stepped gold surfaces. *Surf. Sci.*, 52(1), 21–28. [https://doi.org/10.1016/0039-6028\(75\)90004-7](https://doi.org/10.1016/0039-6028(75)90004-7)
36. Canning, N. D. S. et al. (1984). The adsorption of oxygen on gold. *Surf. Sci.*, 141(1), 240–254. [https://doi.org/10.1016/0039-6028\(84\)90209-7](https://doi.org/10.1016/0039-6028(84)90209-7)
37. Liu, R. (2013). Adsorption and dissociation of H₂O on Au (111) surface: A DFT study. *Comput. Theor. Chem.*, 1019, 141–145. <https://doi.org/10.1016/j.comptc.2013.07.009>
38. Kasemo, B. & Tornqvist, E. (1979). The kinetics of hydrogen interaction with TiH_x films, 0 ≤ x ≤ 2. *Appl. Surf. Sci.*, 3(3), 307–328. [https://doi.org/10.1016/0378-5963\(79\)90002-3](https://doi.org/10.1016/0378-5963(79)90002-3)
39. Wei, F. G. et al. (2004). Precise determination of the activation energy for desorption of hydrogen in two Ti-added steels by a single thermal-desorption spectrum. *Metall. Mater. Trans B*, 35B, 587–597. <https://doi.org/10.1007/s11663-004-0057-x>
40. Iniguez, J. et al. (2007). Vibrational properties of TiH_n complexes adsorbed on carbon nanostructures. *Chem. Phys. Lett.*, 444(1–3), 140–144. <https://doi.org/10.1016/j.cplett.2007.06.133>
41. Wang, R. & Fan, H. (2017). The mechanism of H₂ and H₂O desorption from bridging hydroxyls of a TiO₂(110) surface. *Catal. Sci. Technol.*, 7, 251–264. <https://doi.org/10.1039/C6CY02007K>
42. Koval, I. P. et al. (2015). Interaction of molecular oxygen with Si(001) surface covered with a chromium or titanium monolayer. *Ukr. J. Phys.*, 60(1), 46–51. <https://doi.org/10.15407/ujpe60.01.0046>
43. Niemeyer, T. C. et al. (2002). Activation energy measurement of oxygen ordering in a Nb-Ti alloy by anelastic relaxation. *Mater. Res.*, 5, 143–147. <https://doi.org/10.1590/S1516-14392002000200010>
44. He, J. et al. (2014). Atomic oxygen diffusion on and desorption from amorphous silicate surfaces. *Phys. Chem. Chem. Phys.*, 16, 3493–3500. <https://doi.org/10.1039/C3CP54328E>